Published in final edited form as:
Glia. 2012 December ; 60(12): 2018–2026. doi:10.1002/glia.22416.

Molecular scaffolds underpinning macroglial polarization: an analysis of retinal Müller cells and brain astrocytes in mouse

Rune Enger[1,2,*], **Georg Andreas Gundersen**[1,2,*], **Nadia Nabil Haj-Yasein**[1,2], **Martine Eilert-Olsen**[1,2], **Anna Elisabeth Thoren**[1], **Gry Fluge Vindedal**[2], **Pétur Henry Petersen**[3], **Øivind Skare**[4], **Maiken Nedergaard**[5], **Ole Petter Ottersen**[2], and **Erlend A. Nagelhus**[1,2,5,6]

[1]Centre for Molecular Biology and Neuroscience, Institute of Basic Medical Sciences, University of Oslo, 0317 Oslo, Norway [2]Centre for Molecular Medicine Norway, Nordic EMBL Partnership, University of Oslo, 0318 Oslo, Norway [3]Biomedical Center, Department of Anatomy, Faculty of Medicine, University of Iceland, 101 Reykjavík, Iceland [4]National Institute of Occupational Health, 0033 Oslo, Norway [5]Division of Glial Disease and Therapeutics, Center for Translational Neuromedicine, Department of Neurosurgery, University of Rochester Medical Center, Rochester, New York 14642 [6]Department of Neurology, Oslo University Hospital, Rikshospitalet, 0027 Oslo, Norway

Abstract

Key roles of macroglia are inextricably coupled to specialized membrane domains. The perivascular endfoot membrane has drawn particular attention, as this domain contains a unique complement of aquaporin-4 (AQP4) and other channel proteins that distinguishes it from perisynaptic membranes. Recent studies indicate that the polarization of macroglia is lost in a number of diseases, including temporal lobe epilepsy and Alzheimer's disease. A better understanding is required of the molecular underpinning of astroglial polarization, particularly when it comes to the significance of the dystrophin associated protein complex (DAPC). Here we employ immunofluorescence and immunogold cytochemistry to analyze the molecular scaffolding in perivascular endfeet in macroglia of retina and three regions of brain (cortex, dentate gyrus and cerebellum), using AQP4 as a marker. Compared with brain astrocytes, Müller cells (a class of retinal macroglia) exhibit lower densities of the scaffold proteins dystrophin and α-syntrophin (a DAPC protein), but higher levels of AQP4. In agreement, depletion of dystrophin or α-syntrophin – while causing a dramatic loss of AQP4 from endfoot membranes of brain astrocytes – had only modest or insignificant effect, respectively, on the AQP4 pool in endfoot membranes of Müller cells. Also, while polarization of brain macroglia was less affected by dystrophin depletion than by targeted deletion of α-syntrophin, the reverse was true for retinal macroglia. These data indicate that the molecular scaffolding in perivascular endfeet is more complex than previously assumed and that macroglia are heterogeneous with respect to the mechanisms that dictate their polarization.

Corresponding author: Erlend A. Nagelhus, MD, PhD, Centre for Molecular Medicine Norway, Nordic EMBL Partnership, University of Oslo, P.O. Box 1137 Blindern, N-0318 Oslo, Norway. e.a.nagelhus@ncmm.uio.no, Phone: +47 91736316.
*These authors contributed equally

Keywords

AQP4; aquaporin; dystrophin; endfeet; glia; mdx3cv; syntrophin

Introduction

Our views of macroglial cells have changed dramatically over the past few decades, kindled by a series of breakthroughs in the field of glia research (Barres, 2008;Kimelberg and Nedergaard, 2010). Among the notable discoveries is the realization that macroglial cells are polarized, in the sense that different membrane domains are specialized in terms of function and molecular organization. The perivascular endfeet serve as a case in point. These endfeet – formed by macroglial processes – are endowed with the dystrophin associated protein complex (DAPC) that is now considered a key molecular correlate for functional specialization. Thus, by serving as a multivalent anchor the DAPC may orchestrate a unique molecular assembly and assign a distinct functional role to the membrane domain in question (Amiry-Moghaddam and Ottersen, 2003).

The DAPC is found in many tissues and plays multifarious roles (Le et al., 2010; Waite et al., 2009). In macroglia, the DAPC was found to tether AQP4 to perivascular endfoot membranes through an interaction between the AQP4 C-terminal SXV sequence and α-syntrophin (Neely et al., 2001; Amiry-Moghaddam and Ottersen, 2003). There is also evidence that DAPC is involved in the anchoring of the inwardly rectifying K^+ channel Kir4.1 and possibly a number of other molecules that remain to be identified (Connors and Kofuji, 2002; Connors et al., 2004; Dalloz et al., 2003). Thus, the specific targeting of the DAPC has been invoked to explain the very high K^+ conductances in endfoot membranes and the large water flux that these membranes afford in the build-up phase of a cerebral edema (Amiry-Moghaddam and Ottersen, 2003).

While the DAPC complex has been invoked in macroglial polarization, the relative contribution of different scaffolding proteins remains to be determined. Also, it is not clear whether the scaffolding mechanisms are largely uniform or whether they differ across types of macroglia. Here we employ immunofluorescence and quantitative immunogold analyses to assess whether depletion of dystrophin and α-syntrophin differentially affect macroglial polarization, using AQP4 as a marker and comparing macroglia in three regions of brain (protoplasmic astrocytes of cortex, radial glia of dentate gyrus, and Bergmann glia of cerebellum) with retinal Müller cells.

Materials and Methods

Animals

Male C57BL6/J, B6Ros.Cg-*Dmd*$^{mdx\text{-}3Cv}$/J (*mdx*^{3Cv}; The Jackson Laboratory, Bar Harbor, ME) (Cox, Phelps, Chapman, and Chamberlain, 1993), and B6.129P2-*Snta1*^{tm1Scf} (*α-syntrophin*$^{-/-}$ mice) (Adams et al., 2000) at 8–12 weeks of age were used in this study. The animals were allowed ad libitum access to food and drinking water. For immunofluorescence and quantitative immunogold analysis 4 animals of each genotype

were analyzed. All experiments were approved by the institution's Animal Care and Use Committee.

Antibodies

We used rabbit affinity-purified polyclonal antibodies against dystrophin (Dys331) (Kramarcy et al., 1994), α-syntrophin (Syn259) (Peters et al., 1997), CD31 (BD Pharmingen, San Diego, CA), and AQP4. Two different antibodies towards AQP4 were used: (1) antibody raised against AQP4 C-terminus (Millipore, Billerica, MA; for immunofluorescence), and (2) antibody raised against amino acid residues 249–323 (Sigma, St. Louis, MO; for immunogold cytochemistry).

Immunocytochemistry

Animals were deeply anesthetized by an i.p. injection of a mixture of chloral hydrate, magnesium sulfate, and pentobarbital (142, 70, and 32 mg/kg, respectively). Retinae and brain tissue were fixed by transcardiac perfusion (~10 ml/min) with 0.2% dextran (MW 70,000) in phosphate buffer (PB), followed by either phosphate-buffered 4% formaldehyde, pH 7.4, or bicarbonate-buffered 4% formaldehyde, pH 6.0, followed by 4% formaldehyde, pH 10.5 ("pH shift protocol"; 0.2% picric acid was added to both solutions) (Nagelhus et al., 1998).

Light microscopic immunocytochemistry

Light microscopic immunocytochemistry was performed by using a method of indirect immunofluorescence. The concentrations of the antibodies were: Dys331, 6 μg/ml, Syn259, 1.2 μg/ml; anti-CD31, 2.5 μg/ml; anti-AQP4, 2 μg/ml. Antibodies were diluted in 0.01 M PB with 3% normal goat serum, 1% bovine serum albumin, 0.5% Triton X-100, and 0.05% sodium azide, pH 7.4. The primary antibodies were revealed by a carboxymethylindocyanine (Cy3) or (Cy5)-coupled donkey secondary antibody (1:1,000: Jackson ImmunoResearch Laboratories, Inc., West Grove, PA). Secondary antibodies were diluted in the same solution as the primary antibodies with the omission of sodium azide. Sections of retina and brain were viewed and photographed with a Zeiss LSM 5 Pascal confocal microscope (Carl Zeiss GmbH, Oberkochen, Germany). Sections from brain and retina of all genotypes were run in the same experiment to ensure comparable data. Furthermore all micrographs were as far as possible acquired with the same settings.

Electron microscopic immunocytochemistry and morphological analysis

For immunogold cytochemistry, small blocks of the eyecup and the parietal cortex were subjected to freeze substitution and infiltration in Lowicryl HM20 resin (Polysciences Inc., Warrington, PA, Cat 15924) (Schwarz and Humbel, 1989), before labeling with primary and secondary antibodies. Sections were incubated sequentially in the following solutions (at room temperature): (1) 50 mM glycine in Tris buffer (5 mM) containing 0.01% Triton X-100 and 50 mM NaCl (TBST; 10 min); (2) 0.2% milk powder in TBST (10 min); (3) primary antibody (anti-AQP4 from Sigma, 1.5 μg/ml; anti-α-syntrophin, 12 μg/ml) diluted in the solution used in the preceding step (overnight); (4) same solution as in step 2 (10 min × 2); (5) gold-conjugated IgG (GAR15 nm for AQP4; GAR10 nm for α-syntrophin, Abcam,

Cambridge, UK), diluted 1:20 in TBST containing milk powder and polyethylene glycol (0.5 mg/ml, 1 h). Finally, the sections were counterstained and examined in a FEI Tecnai 12 transmission electron microscope (FEI Company, Hillsboro, OR).

Detection and quantification of gold particles

Digital images were sampled from capillaries in the outer plexiform layer of the retina and in parietal cortex. The number of images taken from each animal ranged from18 to 29 for α-syntrophin labeling and from 31 to 41 for AQP4 labeling. The images were recorded at a nominal magnification of x43000 in 2048 × 2048 × 8 bit. The images were acquired with a commercially available image analysis software (analySIS; Soft Imaging Systems GmbH, Münster, Germany). We used a version of the program that has been modified for acquisition of high-resolution digital images to enable semiautomatic evaluation of immunogold-labeled membranes. Membrane segments of interest were drawn in the overlay and assigned a type label. Gold particles in proximity to each membrane-curve were detected semiautomatically, and the distance between each particle's center of gravity and its membrane curve was calculated by the program. Particles localized within 23 nm from their membrane curve were included in the automated calculation of the number of particles per unit length of membrane (linear particle density). All images, with associated curves, particles, and measurements, were saved to allow later verification and correction. The analyzer was blind to genotype. The measurements were exported to the SPSS 16.0 for Windows software package (SPSS Inc, Chicago, IL, USA), for survey and quality control.

Statistical analysis of immunogold data—We used Poisson mixed models for the analyses of the gold particle counts (Albert, 1999). These models take into account the dependency between observations by including nested variance terms. For the AQP4 immunogold data, three variance terms were included, one for between animal variation, one for between membrane domain variation, and one for within membrane domain variation; while for the α-syntrophin data, two variance terms were added for between animal variation and within animal variation. These models were analysed by the R function glmer in the lme4 package, which for the α-syntrophin analysis gave us estimated differences in linear particle density between tissue groups (wild-type brain, wild-type retina, *α-syntrophin*$^{-/-}$ retina) with corresponding *P* values. For the AQP4 immunogold data we got estimated differences between tissue groups (tissue from brain and retina of wild-types, *mdx*^{3Cv}, and *α-syntrophin*$^{-/-}$ mice) for each macroglial membrane domain (perivascular endfoot membrane and membrane facing neuropil). In the AQP4 analysis we allowed the within membrane variation to differ between membranes. The chosen model structures were based on likelihood ratio tests.

Results

Heterogeneous expression of dystrophin and α-syntrophin within macroglia

In cortex of wild-type mice strong immunofluorescence labeling for dystrophin was observed along the pial surface and around vessels of all calibers (Fig. 1A). Double labeling with the endothelial marker CD31 showed that the dystrophin immunosignal was peripheral to the endothelium, consistent with labeling of astrocytic endfeet (inset, Fig. 1A). The

dentate gyrus (Fig. 1E), cerebellum (Fig. 1I) and cortex displayed the same pattern of dystrophin labeling The perivascular dystrophin signal was notably weaker in retina (Fig. 1M) than in the three regions of brain (Fig. 1A,E,I). Absence of dystrophin immunolabeling in dystrophin-deficient *mdx*^{3Cv} mice confirmed the selectivity of antibodies (Fig. 1B,F,J,N).

The pattern of α-syntrophin immunofluorescence in cortex, dentate gyrus and cerebellum of wild-type mice mimicked that of dystrophin immunofluorescence (Fig. 1C,G,K). Co-immunostaining with antibodies against CD31 indicated α-syntrophin labeling over perivascular astrocytic endfeet (insets in Fig. 1C,G,K). Labeling was absent in *α-syntrophin*$^{-/-}$ mice, attesting to antibody selectivity (Fig. 1D,H,L). In retinae of wild-type mice, α-syntrophin antibodies produced a rather weak and diffuse immunostaining (Fig. 1O). Sections from *α-syntrophin*$^{-/-}$ mice were used as reference (Fig. 1P). In retina, the perivascular α-syntrophin signal was discontinuous and much weaker than that observed in the three regions of brain (compare insets in Fig. 1C,G,K with insets in Fig. 1O).

Immunogold labeling for α-syntrophin was performed on tissue fixed for preservation of antigenicity ("pH-shift fixation protocol") (Nagelhus et al., 1998). Since the pattern of α-syntrophin immunofluorescence was similar in the three regions of brain we restricted the electron microscopical analysis to cortex and retina. In cortex of wild-type mice we observed a distinct immunogold signal over perivascular astrocytic endfoot membranes (Fig. 2A). In retinae from the same mice the signal over Müller cell endfoot membranes was much weaker (Fig. 2C), to the extent of being indistinguishable from background labeling in *α*-syntrophin$^{-/-}$ mice (Fig. 2B,D). Thus, even with optimum sensitivity offered by the pH-shift protocol, the immunogold procedure fails to pick up the pool of α-syntrophin detected by standard immunofluorescence. Consistent with the immunofluorescence data, quantitative analysis of immungold labeling density revealed a strong α-syntrophin signal over perivascular endfoot membranes in cortex (Fig. 2B). Analysis of the distribution of gold particles along an axis perpendicular to the membrane revealed a distinct peak corresponding to the endfoot membrane (inset in Fig. 2A).

Differential contribution of DAPC scaffolding proteins to macroglial polarization in brain and retina

The AQP4 signal intensity in endfeet was used as a proxy of macroglial polarization. In cerebral cortex, dentate gyrus, cerebellum and retina of wild-type mice strong AQP4 immunofluorescence was found around blood vessels of all calibers (Fig. 3A,D,G,J). Co-immunolabeling with antibodies against CD31 confirmed that the AQP4 immunosignal was peripheral to the endothelium, corresponding to macroglial endfeet (insets in Fig. 3A,D,G,J). In cortex, dentate gyrus and cerebellum of *mdx*^{3Cv} and *α-syntrophin*$^{-/-}$ mice, perivascular AQP4 immunofluorescence was much reduced compared to wild-types (Fig. 3A–I), whereas in retina of the same mutants the AQP4 labeling was indiscriminable from that of wild-types (Fig. 3J–L).

In cortex and retina of wild-type mice immunogold cytochemistry showed a polarized distribution of AQP4, with >10 fold higher density of gold particles over macroglial endfoot membranes abutting capillaries than over those facing neuropil (Fig. 4A,D). This is in line with earlier reports (Nielsen et al., 1997; Nagelhus et al., 1998). In cortex of *mdx*^{3Cv} and *α-*

syntrophin$^{-/-}$ mice the AQP4 immunoreactivity over perivascular astrocytic endfoot membranes was reduced by 65% and 88%, respectively, compared to that of wild-types (Fig. 4A–C, G). Lack of dystrophin was associated with 2-fold higher AQP4-signal in perivascular membranes than in those facing neuropil, while deletion of *α-syntrophin* completely abolished AQP4 polarization in astrocytes (Fig. 4G).

The density of gold particles signaling AQP4 over perivascular endfoot membranes of retinal Müller cells was ~70% higher than over those of cortical astrocytes (14.23±0.35 versus 8.27±0.38, P<0.001; Fig. 4A,D,G). In contrast to the situation in brain, the AQP4 immunogold signal over Müller cell endfoot membranes was reduced by only 35% in *mdx*^{3Cv} mice (Fig. 4D,E), and not significantly affected in *α-syntrophin*$^{-/-}$ mice (Fig. 4D,F,G). Thus, in retina of *mdx*^{3Cv} and *α-syntrophin*$^{-/-}$ mice macroglial AQP4 polarization was largely intact, with AQP4 labeling over perivascular endfoot membranes being 6- and 8-fold higher than over those facing neuropil, respectively (Fig. 4G). In retinae of *α-syntrophin*$^{-/-}$ mice the AQP4 labeling of perivascular endfoot membranes was higher than that of *mdx*^{3Cv} mice, whereas in cortex the situation was reversed (Fig. 4G).

Discussion

Loss of macroglial polarization – characterized by depletion of molecules that normally are enriched in macroglial endfoot membranes - emerges as a prominent feature of a number of diseases and disease models, including temporal lobe epilepsy, Alzheimer's disease, stroke, injury, and glioblastoma (Eid et al., 2005; Yang et al., 2011; Noell et al., 2012; Zeynalov et al., 2008; Robel et al., 2011). Losing polarity implies loss of normal function. Notably, regulation of water transport and $[K^+]_o$ appears to be critically dependent on the differential distribution of channel molecules between glial membrane domains (Amiry-Moghaddam and Ottersen, 2003). This raises the question of how specific channel molecules are targeted to and anchored in endfoot membranes.

The present data point to a hitherto unrecognized complexity in molecular scaffolding. Extrapolating from our comparative analysis of cortical astrocytes and retinal Müller cells, we conclude that the densities of the scaffold proteins dystrophin and α-syntrophin show pronounced differences across macroglial subtypes and that the relative importance of these scaffold proteins varies in terms of their contribution to macroglial polarization.

Our finding that dystrophin and α-syntrophin are expressed at far lower concentrations in retina than in cerebral cortex, dentate gyrus and cerebellum could easily be accounted for if Müller cells are less polarized than the brain macroglia (protoplasmic and radial astroglia) used for comparison. To address this possibility, we included a quantitative immunogold analysis of AQP4. Using AQP4 as a "marker" of macroglial polarization, we found no significant difference between Müller cells and cortical astrocytes. In fact, the AQP4 immunogold signal turned out to be *stronger* in retinal endfeet than in cortical endfeet. Taken together, the present analysis indicates that dystrophin and α-syntrophin contribute far less to the polarization of Müller cells than they do to the polarization of brain astrocytes. An earlier study similarly identified a residual AQP4 immunosignal in Müller cell endfeet after deletion of *α-syntrophin* (Puwarawuttipanit et al., 2006). Differences in sampling

procedure and immunolabeling protocol might explain why the present study disclosed an even stronger residual signal than did the study of Puwarawuttipanit et al. (2006).

Macroglia also differ in regard to the relative contribution of the two scaffolding proteins dystrophin and α-syntrophin. Specifically, while polarization of brain macroglia was less affected in *mdx*^{3Cv} mice than in mice lacking α-syntrophin, the opposite was true for retinal macroglia. *Mdx*^{3Cv} mice harbor a mutation that causes a loss of all dystrophin isoforms, including the DP71 isoform that is prevalent in CNS (Cox et al., 1993; Culligan et al., 2001). However, the loss can be partly compensated for by upregulation of utrophin, a dystrophin homologue (Culligan et al., 2001), and this is the most likely explanation why the polarization of brain macroglia was less affected in *mdx*^{3Cv} mice than in mice lacking α-syntrophin.

What explanation could be put forward to explain the situation in Müller cells, where loss of polarization was *more* pronounced after depletion of dystrophin than α-syntrophin? It is probable that anchoring of AQP4 occurs through two different subsets of DAPCs – one with α-syntrophin as the immediate anchor, and one with a different binding partner for AQP4. Being localized to endfeet (Puwarawuttipanit et al., 2006), β1-syntrophin might substitute for α-syntrophin in subsets of DAPCs. Testing of this hypothesis will have to await the development of mice with appropriate gene deletions.

Dystrophin and α-syntrophin play central roles in the orchestration of plasma membrane molecules in endfoot membranes. However, these proteins are not alone responsible for macroglial polarization, as the present data clearly indicate. Deletion of β1-integrin was recently shown to affect the polarized expression of AQP4 and dystrophin (Robel et al., 2009). Moreover, the upregulation of utrophin following depletion of dystrophin (Fort et al., 2008; Culligan et al., 2001) suggests that the former molecule might contribute to scaffolding in endfoot membranes. Future studies on mouse lines lacking utrophin as well as dystrophin (Li et al., 2010) should address this issue and will yield additional insight in the complex mechanisms that underlie macroglial polarization.

Acknowledgments

We thank Professor Stanley C. Froehner and Research Associate Professor Marv E. Adams, University of Washington, Seattle, for providing *α-syntrophin*$^{-/-}$ mice and antibodies directed against α-syntrophin and dystrophin. Mrs. Bjørg Rieber, Karen Marie Gujord, and Jorunn Knutsen provided expert technical assistance. This work was supported by the Research Council of Norway (NevroNor, and FUGE grants), and by Letten Foundation.

References

Adams ME, Kramarcy N, Krall SP, Rossi SG, Rotundo RL, Sealock R, Froehner SC. Absence of alpha-syntrophin leads to structurally aberrant neuromuscular synapses deficient in utrophin. J Cell Biol. 2000; 150:1385–1398. [PubMed: 10995443]

Albert PS. Longitudinal data analysis (repeated measures) in clinical trials. Stat Med. 1999; 18:1707–1732. [PubMed: 10407239]

Amiry-Moghaddam M, Ottersen OP. The molecular basis of water transport in the brain. Nat Rev Neurosci. 2003; 4:991–1001. [PubMed: 14682361]

Barres BA. The mystery and magic of glia: a perspective on their roles in health and disease. Neuron. 2008; 60:430–440. [PubMed: 18995817]

Connors NC, Adams ME, Froehner SC, Kofuji P. The potassium channel Kir4.1 associates with the dystrophin-glycoprotein complex via alpha-syntrophin in glia. J Biol Chem. 2004; 279:28387–28392. [PubMed: 15102837]

Connors NC, Kofuji P. Dystrophin Dp71 is critical for the clustered localization of potassium channels in retinal glial cells. J Neurosci. 2002; 22:4321–4327. [PubMed: 12040037]

Cox GA, Phelps SF, Chapman VM, Chamberlain JS. New mdx mutation disrupts expression of muscle and nonmuscle isoforms of dystrophin. Nat Genet. 1993; 4:87–93. [PubMed: 8099842]

Culligan K, Glover L, Dowling P, Ohlendieck K. Brain dystrophin-glycoprotein complex: persistent expression of beta-dystroglycan, impaired oligomerization of Dp71 and up-regulation of utrophins in animal models of muscular dystrophy. BMC Cell Biol. 2001; 2:2. [PubMed: 11178104]

Dalloz C, Sarig R, Fort P, Yaffe D, Bordais A, Pannicke T, Grosche J, Mornet D, Reichenbach A, Sahel J, Nudel U, Rendon A. Targeted inactivation of dystrophin gene product Dp71: phenotypic impact in mouse retina. Hum Mol Genet. 2003; 12:1543–1554. [PubMed: 12812982]

Eid T, Lee TS, Thomas MJ, Amiry-Moghaddam M, Bjornsen LP, Spencer DD, Agre P, Ottersen OP, de Lanerolle NC. Loss of perivascular aquaporin-4 may underlie deficient water and K+ homeostasis in the human epileptogenic hippocampus. Proc Natl Acad Sci U S A. 2005; 102:1193–1198. [PubMed: 15657133]

Fort PE, Sene A, Pannicke T, Roux MJ, Forster V, Mornet D, Nudel U, Yaffe D, Reichenbach A, Sahel JA, Rendon A. Kir4.1 and AQP4 associate with Dp71- and utrophin-DAPs complexes in specific and defined microdomains of Muller retinal glial cell membrane. Glia. 2008; 56:597–610. [PubMed: 18286645]

Kimelberg HK, Nedergaard M. Functions of astrocytes and their potential as therapeutic targets. Neurotherapeutics. 2010; 7:338–353. [PubMed: 20880499]

Kramarcy NR, Vidal A, Froehner SC, Sealock R. Association of utrophin and multiple dystrophin short forms with the mammalian M(r) 58,000 dystrophin-associated protein (syntrophin). J Biol Chem. 1994; 269:2870–2876. [PubMed: 8300622]

Le RE, Winder SJ, Hubert JF. Dystrophin: more than just the sum of its parts. Biochim Biophys Acta. 2010; 1804:1713–1722. [PubMed: 20472103]

Li D, Yue Y, Duan D. Marginal level dystrophin expression improves clinical outcome in a strain of dystrophin/utrophin double knockout mice. PLoS One. 2010; 5:e15286. [PubMed: 21187970]

Nagelhus EA, Veruki ML, Torp R, Haug FM, Laake JH, Nielsen S, Agre P, Ottersen OP. Aquaporin-4 water channel protein in the rat retina and optic nerve: polarized expression in Muller cells and fibrous astrocytes. J Neurosci. 1998; 18:2506–2519. [PubMed: 9502811]

Neely JD, Amiry-Moghaddam M, Ottersen OP, Froehner SC, Agre P, Adams ME. Syntrophin-dependent expression and localization of Aquaporin-4 water channel protein. Proc Natl Acad Sci U S A. 2001; 98:14108–14113. [PubMed: 11717465]

Nielsen S, Nagelhus EA, Amiry-Moghaddam M, Bourque C, Agre P, Ottersen OP. Specialized membrane domains for water transport in glial cells: high-resolution immunogold cytochemistry of aquaporin-4 in rat brain. J Neurosci. 1997; 17:171–180. [PubMed: 8987746]

Noell S, Wolburg-Buchholz K, Mack AF, Ritz R, Tatagiba M, Beschorner R, Wolburg H, Fallier-Becker P. Dynamics of expression patterns of AQP4, dystroglycan, agrin and matrix metalloproteinases in human glioblastoma. Cell Tissue Res. 2012; 347:429–441. [PubMed: 22307776]

Peters MF, Adams ME, Froehner SC. Differential association of syntrophin pairs with the dystrophin complex. J Cell Biol. 1997; 138:81–93. [PubMed: 9214383]

Puwarawuttipanit W, Bragg AD, Frydenlund DS, Mylonakou MN, Nagelhus EA, Peters MF, Kotchabhakdi N, Adams ME, Froehner SC, Haug FM, Ottersen OP, Amiry-Moghaddam M. Differential effect of alpha-syntrophin knockout on aquaporin-4 and Kir4.1 expression in retinal macroglial cells in mice. Neuroscience. 2006; 137:165–175. [PubMed: 16257493]

Robel S, Berninger B, Götz M. The stem cell potential of glia: lessons from reactive gliosis. Nat Rev Neurosci. 2011; 12:88–104. [PubMed: 21248788]

Robel S, Mori T, Zoubaa S, Schlegel J, Sirko S, Faissner A, Goebbels S, Dimou L, Götz M. Conditional deletion of beta1-integrin in astroglia causes partial reactive gliosis. Glia. 2009; 57:1630–47. [PubMed: 19373938]

Schwarz H, Humbel BM. Influence of fixatives and embedding media on immunolabelling of freeze-substituted cells. Scanning Microsc Suppl. 1989; 3:57–63. [PubMed: 2694274]

Waite A, Tinsley CL, Locke M, Blake DJ. The neurobiology of the dystrophin-associated glycoprotein complex. Ann Med. 2009; 41:344–359. [PubMed: 19172427]

Yang J, Lunde LK, Nuntagij P, Oguchi T, Camassa LM, Nilsson LN, Lannfelt L, Xu Y, Amiry-Moghaddam M, Ottersen OP, Torp R. Loss of astrocyte polarization in the tg-ArcSwe mouse model of Alzheimer's disease. J Alzheimers Dis. 2011; 27:711–722. [PubMed: 21891870]

Zeynalov E, Chen CH, Froehner SC, Adams ME, Ottersen OP, Amiry-Moghaddam M, Bhardwaj A. The perivascular pool of aquaporin-4 mediates the effect of osmotherapy in postischemic cerebral edema. Crit Care Med. 2008; 36:2634–2640. [PubMed: 18679106]

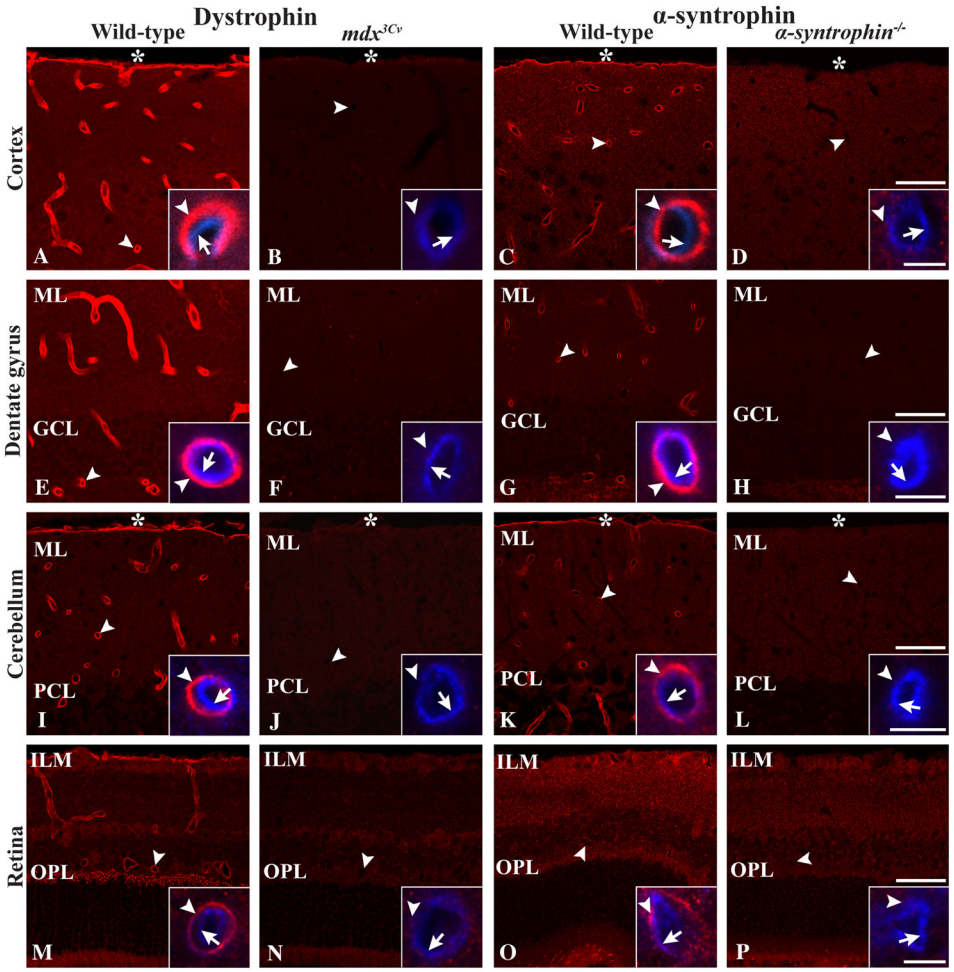

Figure 1.

Immunofluorescence for dystrophin and α-syntrophin in cortex (**A**–**D**), dentate gyrus (**EH**), cerebellum (**I**–**L**) and retina (**M**–**P**). In cortex of wild-type mice strong immunofluorescence signals for dystrophin (**A**) and α-syntrophin (**C**) were seen along the pial surface (asterisks) and around cortical vessels (arrowheads). A similar pattern of immunolabeling was found in dentate gyrus (**E**,**I**) and cerebellum (**G**,**K**) for both antibodies. **Insets:** Co-immunostaining with the endothelial marker CD31 (blue) revealed that labeling for dystrophin and α-syntrophin was peripheral to the endothelium (arrows), corresponding to perivascular macroglial endfeet (arrowheads).The perivascular labeling for dystrophin (**A**,**E**,**I**,**M**) and α-syntrophin (**C**,**G**,**K**,**O**) was much weaker in retina than in the three regions of brain. Loss of immunolabeling in sections obtained from *mdx*^{3Cv} (**B**,**F**,**J**,**N**) and *α-syntrophin*$^{-/-}$ mice (**D**,**H**,**L**,**P**) confirmed the selectivity of the anti-dystrophin and anti-α-syntrophin antibodies, respectively. Scale bars, 50 μm, 5 μm (insets).

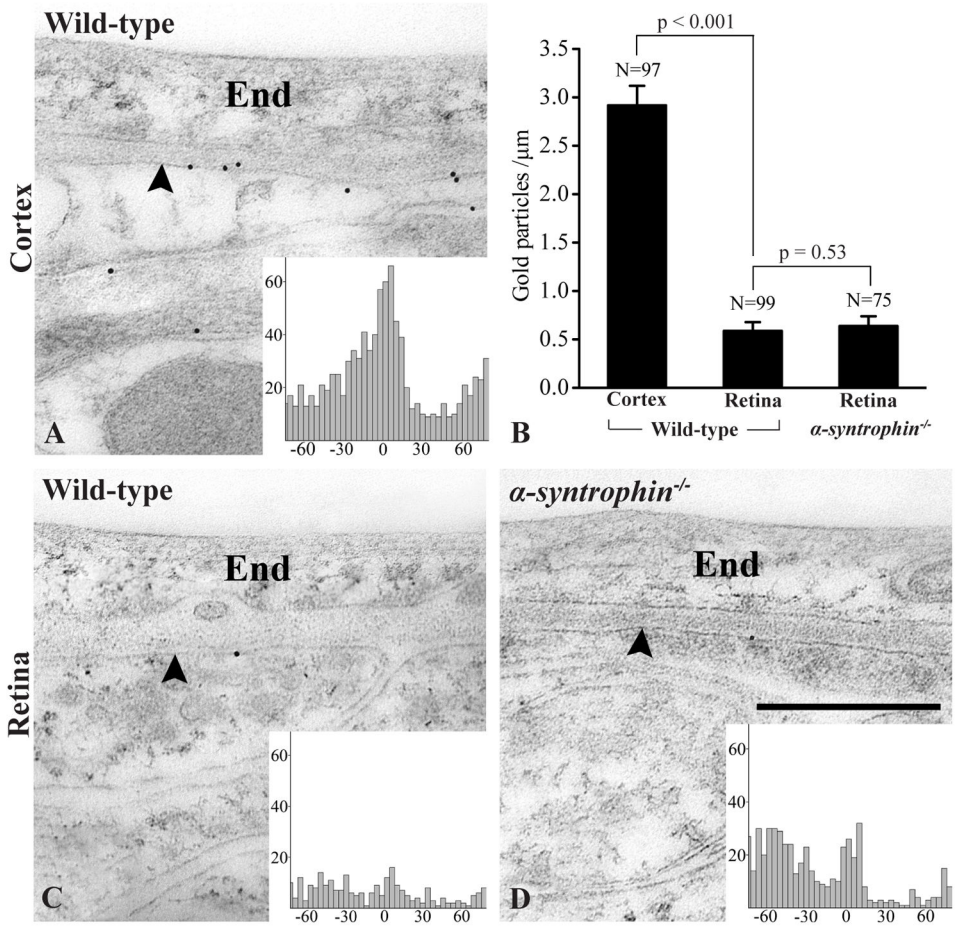

Figure 2.

Subcellular distribution of α-syntrophin in cortex and retina as revealed by immunogold cytochemistry. In wild-type mice gold particles signaling α-syntrophin decorate astrocytic endfoot membranes (arrowheads) peripheral to the endothelium (End) of cortical capillaries (**A**). The immunogold labeling of endfoot membranes (arrowheads) of retinal Müller cells abutting capillaries was very weak in both wild-type (**C**) and *α-syntrophin*$^{-/-}$ mice. **B**: Quantitative analysis of α-syntrophin labeling along perivascular macroglial endfoot membranes in cortex and retina. The ordinate shows number of gold particles per µm of membrane quantified. SEM, number of profiles (N), and p values for comparison are indicated. The α-syntrophin immunogold labeling of wild-type mice was significantly higher over perivascular endfoot membranes of cortical astrocytes than of retinal Müller cells. The latter immunosignal was, however, not significantly different from that of *α-syntrophin*$^{-/-}$ mice, indicating that it was indistinguishable from background labeling. **Insets**: Distribution of gold particles signaling α-syntrophin along an axis perpendicular to the perivascular endfoot membrane. The ordinate indicates number of gold particles per bin (bin width, 4 nm; cytoplasmic side negative). In cortex of wild-type mice a distinct peak is present corresponding to the plasma membrane and its cytoplasmic side, reflecting the localization of α-syntrophin. The gold particle density drops to background level ~30 nm from the midpoint of the membrane, corresponding to the size of the antibody bridge

between the epitope and the corresponding gold particle. No distinct peak is seen over Müller cell endfoot membranes from wild-type and *α-syntrophin*$^{-/-}$ mice, indicating that the signal is unspecific labeling. Scale bar, 0.5 μm.

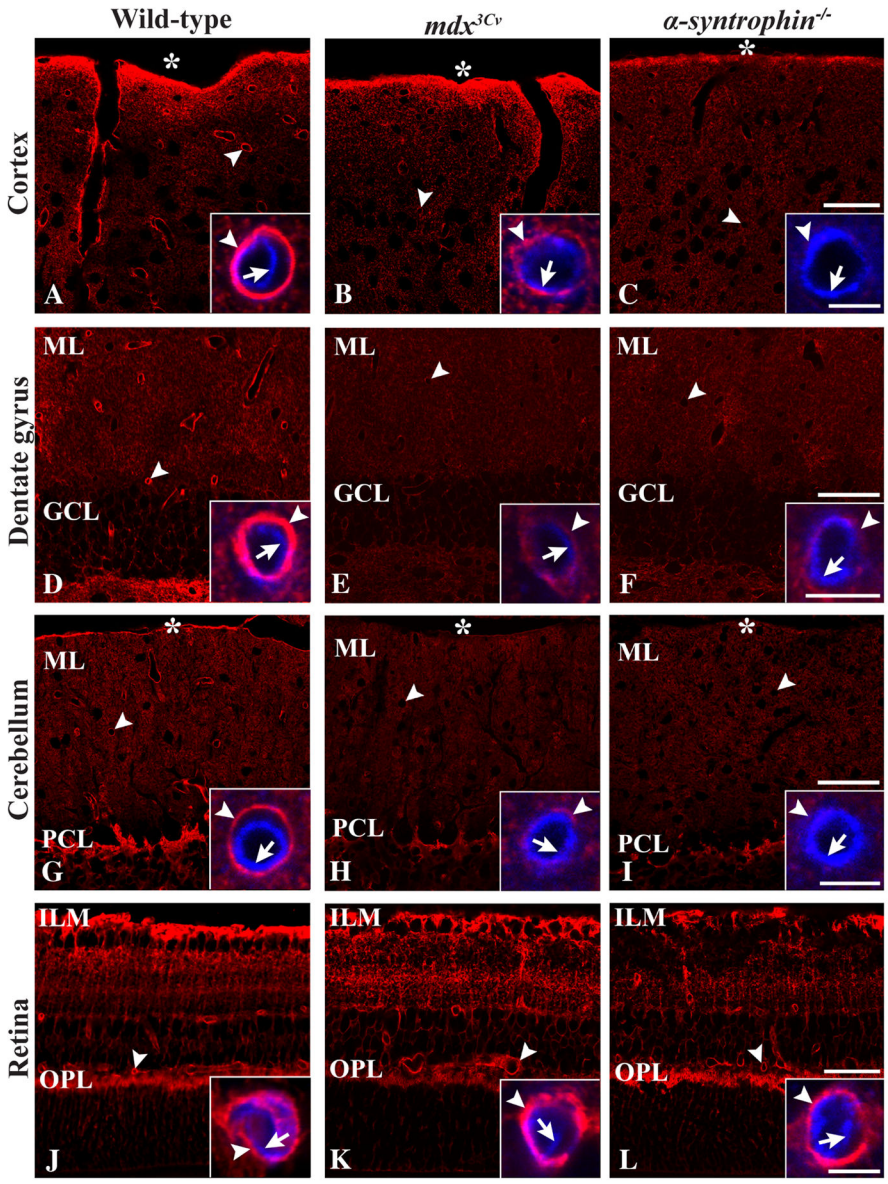

Figure 3.

Distribution of AQP4 immunofluorescence in cortex (**A**–**C**), dentate gyrus (**D**–**F**), cerebellum (**G**–**I**) and retina (**J**–**L**) of wild-type (**A**,**D**,**G**,**J**), *mdx*^{3Cv} (**B**,**E**,**H**,**K**), and *α-syntrophin*$^{-/-}$ mice (**C**,**F**,**I**,**L**). **A**–**C**: In cortex of wild-type mice strong AQP4 labeling was observed around vessels (**A**), whereas in *mdx*^{3Cv} (**B**) and *α-syntrophin*$^{-/-}$ mice (**C**) the perivascular labeling was much weaker. A similar pattern was found in dentate gyrus (**D**–**F**) and cerebellum (**G**–**I**). **J**–**L**: In retina strong perivascular AQP4 labeling (arrowheads) is evident in all genotypes. **Insets**: Double labeling with the endothelial marker CD31 (blue) showed that the AQP4 immunofluorescence was peripheral to endothelial cells (arrows), corresponding to perivascular macroglial endfeet (arrowheads). GCL, granule cell layer; ILM, inner limiting membrane; ML, molecular layer; OPL, outer plexiform layer; PCL, Purkinje cell layer; asterix, pial surface. Scale bars: 50 μm, 5 μm (insets).

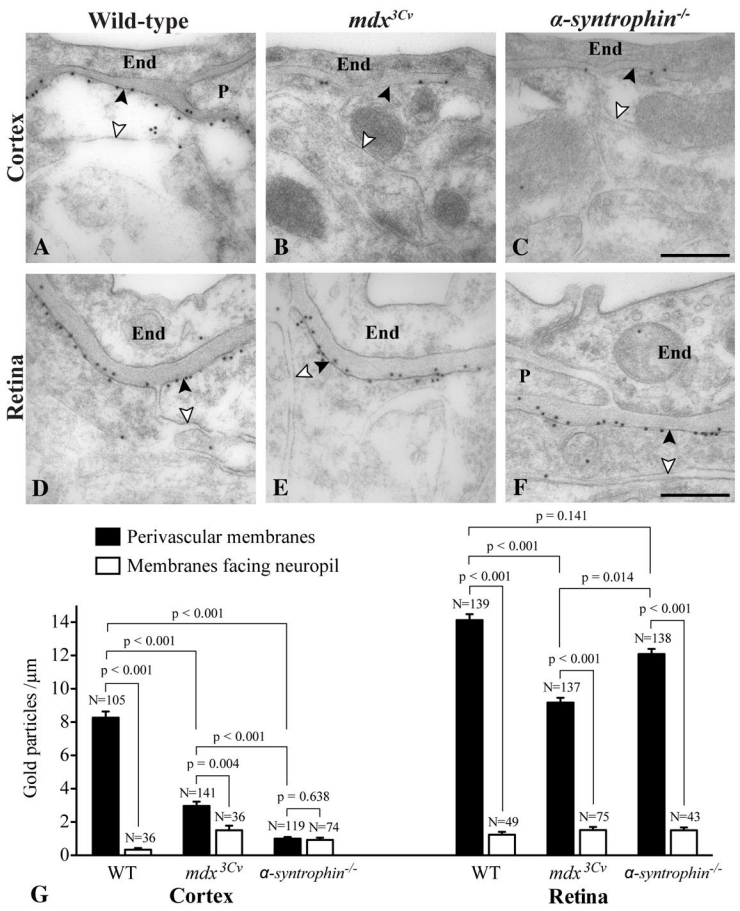

Figure 4.

Electron micrographs showing subcellular distribution of AQP4 immunogold reactivity cortex (**A**–**C**) and retina (**D**–**F**) of wild-type (**A**,**D**), *mdx*^{3Cv} (**B**,**E**) and *α-syntrophin*$^{-/-}$ mice (**C**,**F**). **A**,**D**: In cortex and retina of wild-type mice gold particles signaling AQP4 were much more abundant over macroglial endfoot membranes abutting capillary endothelial cells (End) and pericytes (P) than over macroglial membranes facing neurons (filled and open arrowheads denote the two membrane domains). **A**–**C**: In cortex of *mdx*^{3Cv} and *α-syntrophin*$^{-/-}$ mice AQP4 immunogold reactivity over perivascular endfoot membranes was profoundly reduced compared to those of wild-types. **D**–**F**: In retina, however, AQP4 signaling gold particles were abundant over perivascular endfoot membranes of all genotypes. **G**: Quantitative analysis of AQP4 immunogold labeling over macroglial membranes in cortex and retina of wild-type, *mdx*^{3Cv} and *α-syntrophin*$^{-/-}$ mice. The ordinate shows number of gold particles per µm of membrane quantified. The filled and open bars indicate labeling densities over endfoot membranes abutting capillaries (“Perivascular membranes”) and membranes facing neuropil, respectively (denoted with filled and open arrowheads in **A**–**F**, for easy comparison). SEM, number of profiles (N), and brackets with p values for comparison are indicated (cf. Materials and Methods). Scale bar, 0.5 µm.